MITSUBISHI ELECTRIC RESEARCH LABORATORIES
https://www.merl.com

Efficient Direct Near-Field MIMO Radar Imaging via Multiresolution Image Support Refinement

Oral, Okyanus; Feuillen, Thomas; Mysore Rama Rao, Bhavani Shankar; Wang, Pu

TR2026-160 October 29, 2026

Abstract

Multiple-input multiple-output (MIMO) arrays enable high-resolution radar imaging by synthesizing large effective apertures using spatially distributed transmit and receive antennas. In near-field imaging applications, the resulting multistatic geometry leads to high computational complexity. Consequently, reducing this complexity is of significant interest. To this end, most existing fast near-field MIMO imaging approaches trade reconstruction accuracy for faster runtimes by using lower-complexity approximations of the imaging operator. In this paper, we develop an efficient direct reconstruction approach that achieves the same accuracy as backprojection while prioritizing the early reconstruction of high-energy regions of the scene. Our method is based on partitioning the channels of the MIMO array to concentric apertures with equal resolution improvements. This enables reordering of the backprojection summation for multiresolution image refinement. By storing the backprojected pixel values in a multiresolution tree, we sequentially estimate the energy distribution of the scene and decide on the region to reconstruct next. Simulations show that, compared with standard raster scanning, the proposed approach converges faster to the final backprojection image, allowing earlier recovery of the scene content.

Asilomar Conference on Signals, Systems and Computers (ACSSC) 2026

© 2026 MERL. This work may not be copied or reproduced in whole or in part for any commercial purpose. Permission to copy in whole or in part without payment of fee is granted for nonprofit educational and research purposes provided that all such whole or partial copies include the following: a notice that such copying is by permission of Mitsubishi Electric Research Laboratories, Inc.; an acknowledgment of the authors and individual contributions to the work; and all applicable portions of the copyright notice. Copying, reproduction, or republishing for any other purpose shall require a license with payment of fee to Mitsubishi Electric Research Laboratories, Inc. All rights reserved.

Mitsubishi Electric Research Laboratories, Inc.
201 Broadway, Cambridge, Massachusetts 02139

Efficient Direct Near-Field MIMO Radar Imaging via Multiresolution Image Support Refinement

Okyanus Oral[1], Thomas Feuillen[2], Bhavani Shankar Mysore Rama Rao[1], Pu (Perry) Wang[3]
[1]Interdisciplinary Centre for Security, Reliability and Trust, University of Luxembourg, Luxembourg.
[2]Aetherion Space and Defence, Luxembourg.
[3]Mitsubishi Electric Research Laboratories, Cambridge, MA, USA.

***Abstract*—Multiple-input multiple-output (MIMO) arrays enable high-resolution radar imaging by synthesizing large effective apertures using spatially distributed transmit and receive antennas. In near-field imaging applications, the resulting multistatic geometry leads to high computational complexity. Consequently, reducing this complexity is of significant interest. To this end, most existing fast near-field MIMO imaging approaches trade reconstruction accuracy for faster runtimes by using lower-complexity approximations of the imaging operator. In this paper, we develop an efficient direct reconstruction approach that achieves the same accuracy as backprojection while prioritizing the early reconstruction of high-energy regions of the scene. Our method is based on partitioning the channels of the MIMO array to concentric apertures with equal resolution improvements. This enables reordering of the backprojection summation for multiresolution image refinement. By storing the backprojected pixel values in a multiresolution tree, we sequentially estimate the energy distribution of the scene and decide on the region to reconstruct next. Simulations show that, compared with standard raster scanning, the proposed approach converges faster to the final backprojection image, allowing earlier recovery of the scene content.**

***Index Terms*—Near-field, MIMO, image reconstruction, multiresolution processing.**

I. Introduction

Near-field radar imaging with multiple-input multiple-output (MIMO) arrays involves a multistatic measurement model. As a result, even direct reconstruction methods, such as backprojection, can become prohibitively expensive to compute for high-resolution, large-scale image formation [1]–[8]. Consequently, many works in the literature focus on improving the computational complexity of near-field MIMO radar imaging [1]–[8].

A common strategy to reduce the computational complexity is to relate the spectral content of the scene to the acquired MIMO measurements [2]–[4]. This enables the use of Fast Fourier Transform (FFT) algorithms to reconstruct the image once its spectrum is formed by available measurements. However, these algorithms commonly require high-dimensional interpolations, and the chosen interpolation scheme determines both the quality of the reconstructions and computational efficiency [2]–[4]. Furthermore, methods that use approximated measurement models to achieve lower-complexity imaging operators [5], [6] often suffer from induced phase errors, constraining the imaging region for which their reconstruction quality is acceptable [9]. Another fast reconstruction strategy is to use hierarchical processing with time-domain methods by exploiting the resolution limits of MIMO subapertures [7], [8]. However, to hierarchically combine low-resolution images for high-resolution reconstruction, such methods also require carefully designed interpolation schemes [7], [8], and their effectiveness is prone to the choice of image sampling grids [8] and array partitioning [7].

In this work, we develop a novel near-field MIMO radar imaging method that achieves efficient reconstruction by reordering the backprojection summation. Akin to the adaptive sampling strategies developed for near-field applications to effectively collect measurements [10], [11], our main idea is to prioritize the reconstruction and refinement of salient regions of the scene. To avoid spending compute on empty regions of the scene, we define salient regions as those with high energy. This allows us to terminate the summation iterations earlier based on recovered energy, while guaranteeing that the final backprojection image can be reached at the refinement limit.

The developed method starts from an initial low-resolution reconstruction and sequentially determines the pixels to refine. For this, we partition the MIMO channels to concentric apertures with resolution improvements, which enable the image to be reconstructed at different resolution levels and its refinement without any interpolation steps. This naturally leads to operating on a multiresolution pixel tree, where each node is the reconstructed pixel value at a particular resolution. Consequently, the refinement steps become equivalent to expanding the frontier nodes. Importantly, when the image size and the number of channels are sufficiently large, the developed method retains the same order of computational complexity as the standard backprojection summation.

We demonstrate the effectiveness of our method using simulations and compare it with depth-first and breadth-first summation orders. Our results show that the developed method allows faster convergence to the final backprojection output, enabling higher reconstruction accuracy within the early summation iterations.

OO, BSMRR are supported by the Luxembourg National Research Fund (FNR) through the CORE project METSA under grant C22/IS/17391632. TF was supported by FNR CORE SURF Project, ref C23/IS/18158802/SURF. PW is exclusively supported by MERL.

At the time of this study, TF was with Interdisciplinary Centre for Security, Reliability and Trust, University of Luxembourg; he is now with Aetherion Space and Defence, Luxembourg.

Corresponding author: OO (email: okyanus.oral@uni.lu).

II. Multistatic Imaging

A. Measurement Model

Consider a general near-field MIMO imaging setting where M_t transmit antennas sequentially illuminate the scene to image a target in the near-field of the MIMO array. The reflected echoes are then captured using M_r receive antennas for M_k number of operating frequencies, totaling $M = M_t M_r M_k$ number of measurements.

Assuming that the scene consists of N point scatterers, we can express the corresponding frequency domain measurements as the superpositions of echoes for each scatterer. This corresponds to a linear measurement model which can be expressed as a matrix-vector product as follows,

$$\mathbf{s} = \mathbf{\Phi}\boldsymbol{\sigma}. \tag{1}$$

Here $\mathbf{s} \in \mathbb{C}^M$ denotes the measurement vector in the frequency domain, $\mathbf{\Phi} \in \mathbb{C}^{M\times N}$ denotes the measurement matrix, and $\boldsymbol{\sigma} \in \mathbb{C}^N$ denotes the ground truth reflectivity vector. By denoting the frequency domain measurement for the t-th transmit antenna at position $\mathbf{p}_T^{(t)} \in \mathbb{R}^3$ and r-th receive antenna at position $\mathbf{p}_R^{(r)} \in \mathbb{R}^3$ for the k-th operating frequency, f_k, as $s_k^{(t,r)} \in \mathbb{C}$, we can express the measurement vector as $\mathbf{s} = \mathrm{vec}(s_k^{(t,r)})$ where $\mathrm{vec}(\cdot)$ is the vectorization operator over measurement indices (k, t, and r). Then the n-th column of the measurement matrix, which represents the contribution of the n-th scatterer at position $\mathbf{p}_n \in \mathbb{R}^3$, can be constructed as $\mathbf{\Phi}_{:,n} \triangleq \mathrm{vec}\left(\exp\{-j2\pi f_k \tau_n^{(t,r)}\}\right)$ using the corresponding round trip delay $\tau_n^{(t,r)} \triangleq \frac{1}{c}(\|\mathbf{p}_T^{(t)} - \mathbf{p}_n\|_2 + \|\mathbf{p}_R^{(r)} - \mathbf{p}_n\|_2)$ with c denoting the speed of light.

B. Backprojection Reconstruction

To detect the presence of a target at candidate positions, the backprojection algorithm [8], [12] applies the adjoint of the measurement model in (1). Assuming that the associated main-lobe width and the side-lobe levels of the MIMO array are negligible, the corresponding matrix-vector product with the adjoint matrix yields a scaled version of the scene reflectivity where the processing gain becomes proportional to the number of measurements, i.e. $\mathbf{\Phi}^{\mathsf{H}}\mathbf{\Phi} \approx M\mathbf{I}$. Accordingly, the back-projection result can be used to approximate the reflectivity content as follows,

$$\mathbf{b} = \mathbf{\Phi}^{\mathsf{H}}\mathbf{s} = \mathbf{\Phi}^{\mathsf{H}}\mathbf{\Phi}\boldsymbol{\sigma} \approx M\boldsymbol{\sigma} \implies \hat{\boldsymbol{\sigma}} = \frac{1}{M}\mathbf{b}. \tag{2}$$

where $\mathbf{b}$ is the backprojection image and $\hat{\boldsymbol{\sigma}}$ corresponds to the reflectivity estimate.

To form the backprojection image, we sample the scene coordinates within a region of interest based on the resolution offered by the MIMO array [2]. As a result, the number of scatterers, N, is assumed to equal the number of voxels/pixels in the image. We set the sampling periods in the cross-range by computing the resolutions at the closest voxel/pixel coordinate. For an imaging plane at range $z = z_0$ away from the MIMO array, we approximate the cross-range resolutions along x and y dimensions as [2],

$$\delta_{c,x} \approx \frac{z_0}{L_{T,x} + L_{R,x}}\lambda_{\min} \text{ and } \delta_{c,y} \approx \frac{z_0}{L_{T,y} + L_{R,y}}\lambda_{\min}. \tag{3}$$

Here, $L_{T,x}$, $L_{T,y}$ and $L_{R,x}$, $L_{R,y}$ denote the lengths of transmit and receive antenna arrays along x and y dimensions, respectively, and $\lambda_{\min}$ is the minimum operating wavelength.

The backprojection summation in (2) is commonly implemented in an operator form for efficient computation without forming the adjoint of the measurement matrix [12]. For this, the collected frequency-domain measurements are first converted to range-domain via an FFT, and then an interpolation scheme is used to compute the summation using the range-domain data. The resulting computational complexity is of the order $\mathcal{O}(M_t M_r M_k \log M_k + \alpha N M_t M_r)$ floating point operations, where the coefficient α is determined by the interpolation scheme. As a result, the computational cost of the backprojection operator scales with the product of the number of pixels, N, and the number of channels, $M_t M_r$, which becomes prohibitively large for high-resolution imaging using MIMO arrays with hundreds/thousands of channels [1], [7], [8].

III. Proposed method

We now present the developed multiresolution image support refinement method for efficient direct near-field MIMO radar imaging. We first provide the details on partitioning the MIMO channels to enable the use of a multiresolution tree structure for backprojection reconstruction. Then, we explain the developed image-refinement strategy for the early recovery of high-energy regions of the scene, along with a natural termination criterion. Throughout the section, we calculate the additional computational complexity required to employ the refinement strategy and show that the computational cost will be dominated by backprojection summation for large NM_tM_r.

A. Partitioning Channels Based on Cross-Range Resolution

Here, our goal is to associate the transmit-receive antenna pairs (channels) with a certain resolution. For this, we use an approximate monostatic antenna array equivalent to the MIMO array. Accordingly, a channel can be associated with a certain resolution by the distance of the corresponding approximate transceiver at $\mathbf{p}_c^{(t,r)} \triangleq \frac{1}{2}(\mathbf{p}_T^{(t)} + \mathbf{p}_R^{(r)})$ to the aperture center. This allows us to use monostatic cross-range resolution formulas [12] given by $\delta_{c,x} \approx \lambda_{\min} z_0/(2L_x)$ and $\delta_{c,y} \approx \lambda_{\min} z_0/(2L_y)$, where L_x and L_y denote the aperture sizes of the equivalent monostatic array along the x- and y-dimensions. Although the validity of this monostatic array approximation degrades at short ranges, it still remains a useful approximation to determine the MIMO channels' contribution to the cross-range resolution.

Based on this assumption, we partition the channels of the MIMO array to yield resolution improvements as illustrated in Fig. 1. As seen from the figure, the monostatic equivalent

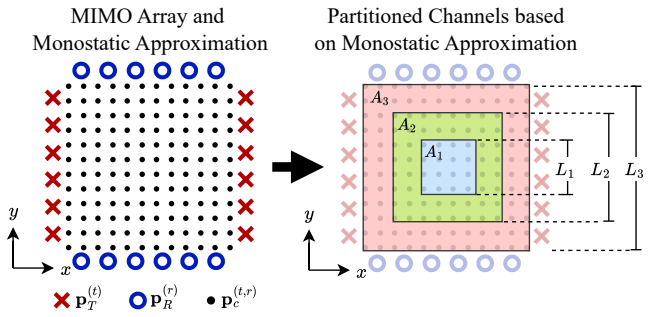

Fig. 1: Schematic diagram of partitioning MIMO channels based on cross-range resolution.

array is partitioned into three concentric apertures, A_1, A_2, and A_3, with increasing widths L_1, L_2, and L_3. As a result, the channels, (t, r), assigned to the apertures A_1, A_2, and A_3, respectively, correspond to the low, medium, and high cross-range resolutions.

B. Multiresolution Tree

The image can now be reconstructed starting from the channels corresponding to the innermost virtual sub-aperture and refined by the inclusion of channels from outer apertures. This corresponds to reconstruction by different resolution levels, where the number of resolution levels, $l_{\max}$, is determined by the number of concentric sub-apertures. As a result, the reconstructed image can be stored and iteratively refined using a multiresolution tree.

Each level (or depth) of the multiresolution tree, indexed by l, corresponds to a different resolution, and each node at a particular level, indexed by n, corresponds to an image pixel at that resolution. The backprojection reconstruction at level l and node n is then found by computing the backprojection summation using all measurements corresponding to subapertures $A_{l'}$ for $l' \in \{1, \ldots, l\}$, and is denoted by $b_{l,n}^{(i)}$ for the i-th refinement iteration. Then, for the reconstructed value of a node at level l and index n at iteration i to be reused without any need for interpolation at next iteration $i+1$ for the child nodes at $l+1$, we constrain the tree structure such that the sampled coordinates are decimated for each parent node by odd numbers. This makes sure that there is a center child node that shares the same coordinate as the low-resolution pixel. Consequently, the value stored at the parent node can be used for the center node to avoid additional processing for that node. As a result, the number of coherent summations required to reach the finest resolution is the same as that of standard backprojection summation.

C. Heuristics for Multiresolution Refinement

1) Node Scoring: To decide which region of the coarse image to refine at the next iteration, we score the nodes at the frontier of the tree based on their energy. This energy score allows us to prioritize the reconstruction of high-energy regions in the image first.

Analogous to the reflectivity estimate for the reflectivity image at the finest resolution in (2), we can define the multiresolution reflectivity estimate at (l, n)-th node at i-th iteration as,

$$\hat{\sigma}_{l,n}^{(i)} \triangleq \frac{b_{l,n}^{(i)}}{\sum_{l'=1}^{l_{\max}} |A_{l'}|} \tag{4}$$

where $|A_l|$ denotes the number of measurements associated with the l-th sub-aperture with $\sum_{l'=1}^{l_{\max}} |A_{l'}| = M$.

We define the score of a frontier node as the energy associated with it on the final image. Accordingly, when computing the score, we account for the total number of pixels it covers on the finest-resolution image. For a frontier node at level l, the corresponding number of pixels on a d-dimensional image is equal to $3^{d(l_{\max}-l)}$. Then the score for a frontier node can be computed as,

$$E_{l,n}^{(i)} \triangleq \begin{cases} |\hat{\sigma}_{l,n}^{(i)}|^2 \, 3^{d(l_{\max}-l)} & , l < l_{\max} \\ 0 & , l = l_{\max} \end{cases}, \tag{5}$$

where we set the score of the nodes at the final level to zero to limit the tree depth to the resolution of the full aperture. This computation adds only $\mathcal{O}(1)$ floating point operations per frontier node. By computing the number of nodes from bottom up using decimations of three for each level, we can bound the total number of nodes as,

$$N_{\text{node}} = \sum_{l=0}^{l_{\max}-1} N 3^{-dl} = N \left(\frac{1 - 3^{-l_{\max}}}{1 - 3^{-d}} \right) < 3^d N. \tag{6}$$

Therefore, computing the frontier scores adds $\mathcal{O}(N)$ computation cost, which will be negligible for large N and $M_t M_r$.

2) Maximum-Score Search: Since the scores are computed and stored for frontier nodes on the multiresolution tree, we use a max-heap to efficiently find the frontier node with the maximum score. At each refinement iteration, this requires 3^d comparisons for each level to determine the maximum score. While constructing the heap, we also propagate the branch indices corresponding to the frontier node with the maximum score. As a result, the cost to locate the frontier node to refine can be assumed to be zero.

The additional computation cost can then be found by multiplying the max-heap cost per iteration by the number of iterations. By using the upper bound for the number of nodes in (6) and the number of child nodes per refinement (3^d), the iteration count can be bounded by,

$$N_{\text{iter}} = \frac{N_{\text{node}}}{3^d} < \frac{N 3^d}{3^d} = N. \tag{7}$$

Accordingly, the additional computation cost summed over all iterations is proportional to the multiplication of the number of comparisons for each level 3^d, the total number of levels $l_{\max}$, and the total number of iterations N_{iter}, and is bounded by $< 3^d l_{\max} N$. At the end, using a max-heap to decide where to refine at each iteration adds an additional computation cost on the order of $\mathcal{O}(N)$, which again will be negligible for a large image size and a high number of MIMO channels.

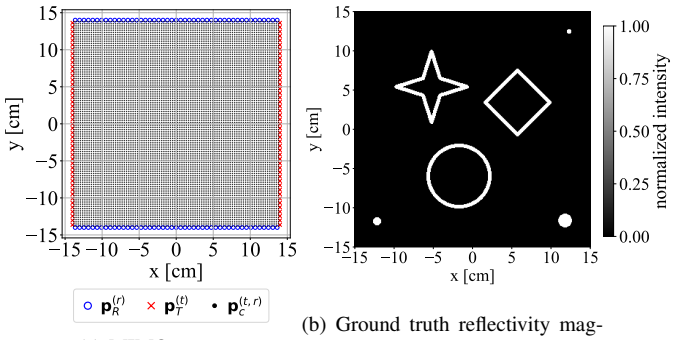

(a) MIMO array.

(b) Ground truth reflectivity magnitudes.

Fig. 2: Simulated MIMO array and the scene.

3) Termination Criteria: A natural criterion to terminate the iterations is to check if the maximum energy score of the frontier nodes decreases below a certain fraction of the total image energy. However, since the image is not known a priori, we use an estimate of the total image energy using the energy of the measurements. We establish this using the matrix norm and the Cauchy-Schwarz inequality as,

$$\|\mathbf{s}\|_2^2 = \|\mathbf{\Phi}\boldsymbol{\sigma}\|_2^2 \leq \|\mathbf{\Phi}\|_2^2 \|\boldsymbol{\sigma}\|_2^2 \implies \frac{\|\mathbf{s}\|_2^2}{\|\mathbf{\Phi}\|_2^2} \leq \|\boldsymbol{\sigma}\|_2^2, \quad (8)$$

where $\|\mathbf{\Phi}\|_2$ denotes the spectral norm of $\mathbf{\Phi}$. Using the assumption in (2), the square of the spectral norm can be approximated as, $\|\mathbf{\Phi}\|_2^2 \approx M$. As a result, we can terminate the refinement iterations using,

$$\max_{(l,n)} E_{l,n}^{(i)} \leq \eta \frac{\|\mathbf{s}\|_2^2}{M} \leq \eta \|\boldsymbol{\sigma}\|_2^2. \quad (9)$$

for some $\eta \in (0, 1)$. The computation cost of this energy bound is $\mathcal{O}(M)$ floating point operations and becomes negligible compared to the cost of backprojection summation for large N and $M_t M_r$.

IV. Results

We investigate the performance of the developed method by simulating a near-field millimeter-wave MIMO radar imaging scenario similar to [11]. The simulated MIMO array is shown in Fig. 2a and is based on the QAR50 submodule from Rohde & Schwarz [13]. The MIMO array consists of 94 transmit and 94 receive antennas and has an aperture width of 15 cm in both the x and y dimensions. The magnitude of the reflectivity values of the simulated two-dimensional scene is shown in Fig. 2b, which lies in the near-field of the MIMO array at the $z_0 = 30$ cm plane. The associated measurements are simulated for 128 linearly spaced frequencies from the $72-82$ GHz band using equation (1).

We partition the channels of the MIMO array into 4 concentric sub-apertures, which results in a multiresolution tree of depth 4. The scene is then sampled at the $z_0 = 30$ cm plane with a $\sim$ 2 mm sampling period, which corresponds to the cross-range resolution computed using (3). Given the sampling period and the multiresolution tree structure, the number of pixels in the image is set to the smallest integer that covers the 30 cm sidelength of the region of interest, resulting in an image of size 162×162.

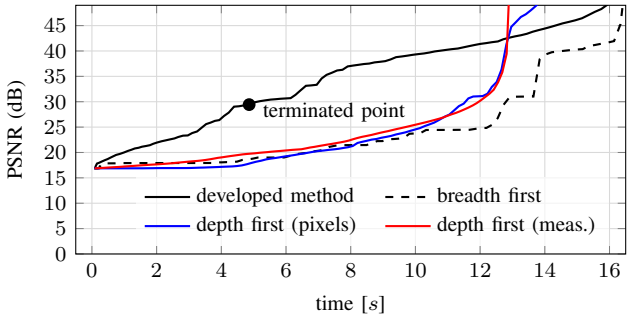

Fig. 3: PSNR with respect to runtime.

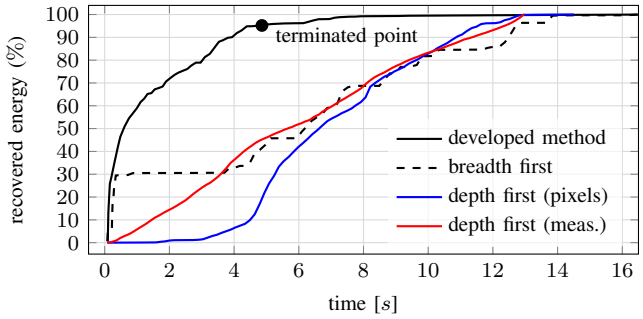

Fig. 4: Recovered energy with respect to runtime.

A. Effect of Backprojection Summation Order

We compare the convergence speed of the developed backprojection summation method with respect to depth-first and breadth-first summation orders. Specifically, we define depth-first on pixels as computing a single pixel using all measurements, and depth-first on measurements as iterating over measurements to accumulate contributions across all image pixels. On the other hand, breadth-first refers to processing on the multiresolution tree level by level.

To quantitatively evaluate the performance at any summation iteration, we convert the frontier nodes of the multiresolution tree to the equivalent raster image on a full-resolution grid. Denoting the corresponding raster image for the i-th iteration as $\mathbf{b}^{(i)}$, we record the recovered image energy with respect to iterations as $\|\mathbf{b}^{(i)}\|_2^2 / \|\mathbf{b}\|_2^2$. Similarly, we compute the peak signal-to-noise ratio (PSNR) [14] using the oracle, $\mathbf{b}$, and $\mathbf{b}^{(i)}$ at any given iteration. The PSNR and recovered energy with respect to the runtimes of different backprojection summations are shown in Fig. 3 and Fig. 4, respectively. All results are computed on an AMD Ryzen 7 7840HS CPU using Python. To terminate the iterations of the developed method, we use $\eta = 10^{-6}$ in (9).

As seen from the iterations, the developed method converges to the final backprojection result faster than the other summation orders. In particular, while the summations with depth-first ordering take around 13 seconds, the developed

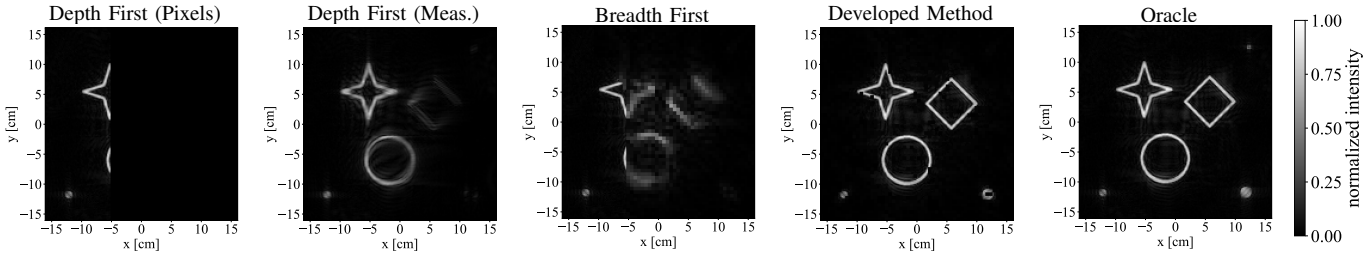

(a) 18.2 dB (26.0%) (b) 19.8 dB (46.3%) (c) 19.0 dB (45.7%) (d) 29.4 dB (95.2%) (e) $+\infty$ dB (100%)

Fig. 5: The reconstructions at the termination point are shown in (a)-(d) while the oracle reconstruction is shown in (e). The PSNR and the recovered energy (in parentheses) are indicated below each reconstruction.

method terminates about 2.5 times earlier at 4.86 seconds. As a result, it achieves a high PSNR of 29.4 dB, which is more than 9 dB higher than the reconstructions from the other summation orders at the same runtime. Similarly, while the recovered energy percentages with other summation orders are all below 50%, the developed method recovers 95.2% of the oracle image's energy at the termination point.

The oracle backprojection image and the reconstructions terminated within the same time budget as the developed method are shown in Fig. 5. As seen, the medium-sized disk at the bottom-right of the scene is recovered only by the developed method within the time budget. Nevertheless, we also see that the small disk at the top-right is still missing, as expected, since the frontier nodes associated with that region will have a low energy throughout the iterations. Importantly, while the other methods take a longer time to recover the three shapes in the middle of the scene due to their orientation and/or position, all three shapes are clearly identifiable with the developed method.

These results demonstrate that the developed multiresolution support-refinement strategy, combined with the energy-based termination criterion, enables early termination and reduced computation while recovering most of the scene's high-energy content, leading to accurate early reconstructions.

V. Conclusion

In this paper, we developed a novel near-field MIMO radar imaging method that prioritizes the early reconstruction of high-energy regions of the scene. This is achieved by partitioning the MIMO channels to concentric apertures with resolution improvements, which allows image refinement on a multiresolution tree based on pixel energy. The developed method guarantees refinement steps to convergence to the backprojection output while retaining the same order of computational complexity for a high number of channels and large image sizes. The simulations demonstrate the effectiveness of the developed method, in which the summation iterations converge faster to the final backprojection image than with depth-first or breadth-first summation orders.

References

[1] A. M. Molaei, S. Hu, V. Fusco, T. Fromenteze, R. Kumar, M. A. B. Abbasi, and O. Yurduseven, "Advanced near-field radar imaging approaches in security: An overview on signal processing challenges, opportunities, and future directions," *IEEE Signal Processing Magazine*, vol. 42, no. 1, pp. 126–146, 2025.

[2] X. Zhuge and A. G. Yarovoy, "Three-dimensional near-field MIMO array imaging using range migration techniques," *IEEE Transactions on Image Processing*, vol. 21, no. 6, pp. 3026–3033, 2012.

[3] J. Wang, P. Aubry, and A. Yarovoy, "3-D short-range imaging with irregular MIMO arrays using NUFFT-based Range Migration Algorithm," *IEEE Transactions on Geoscience and Remote Sensing*, vol. 58, no. 7, pp. 4730–4742, 2020.

[4] T. Fromenteze, O. Yurduseven, F. Berland, C. Decroze, D. R. Smith, and A. G. Yarovoy, "A transverse spectrum deconvolution technique for MIMO short-range Fourier imaging," *IEEE Transactions on Geoscience and Remote Sensing*, vol. 57, no. 9, pp. 6311–6324, 2019.

[5] S. Gui, Y. Li, H. Nie, Z. Zhao, L. Fan, and Z. Tian, "3D near-field fast imaging method for MMW MIMO array radar," in *2024 IEEE International Conference on Signal, Information and Data Processing (ICSIDP)*, 2024, pp. 1–5.

[6] W. F. Moulder, J. D. Krieger, J. J. Majewski, C. M. Coldwell, H. T. Nguyen, D. T. Maurais-Galejs, T. L. Anderson, P. Dufilie, and J. S. Herd, "Development of a high-throughput microwave imaging system for concealed weapons detection," in *2016 IEEE International Symposium on Phased Array Systems and Technology (PAST)*, 2016, pp. 1–6.

[7] T. Song, X. Yao, L. Wang, Y. Wang, and G. Sun, "Fast Factorized Kirchhoff Migration Algorithm for near-field radar imaging with sparse MIMO arrays," *IEEE Transactions on Geoscience and Remote Sensing*, vol. 62, pp. 1–14, 2024.

[8] R. Zhu, J. Zhou, S. Chen, and H. Ding, "Pseudo-Trapezoidal Fast Factorized Backprojection Algorithm for near-field sparse MIMO array 3-D imaging," *IEEE Transactions on Aerospace and Electronic Systems*, 2025.

[9] N. E. Doren, *Space-variant post-filtering for wavefront curvature correction in polar-formatted spotlight-mode SAR imagery*. The University of New Mexico, 1999.

[10] R. Rafiee Alavi, R. Mirzavand, A. Kiaee, and P. Mousavi, "An adaptive data acquisition technique to enhance the speed of near-field antenna measurement," *IEEE Transactions on Antennas and Propagation*, vol. 70, no. 7, pp. 5873–5883, 2022.

[11] M. Brinkmann, M. M. Saurer, G. F. Hamberger, and T. F. Eibert, "Adaptive sampling for efficient synthetic aperture radar imaging," in *2025 22nd European Radar Conference (EuRAD)*, 2025, pp. 174–177.

[12] M. Soumekh, *Synthetic aperture radar signal processing with MATLAB algorithms /*. New York: John Wiley Sons, 1999. [Online]. Available: https://proxy.bnl.lu/login?url=https://learning.oreilly.com/library/view/~/9780471297062/?ar&orpq&email=^u

[13] Rohde & Schwarz, "R&S QAR50 Quality Automotive Radome Tester," https://www.rohde-schwarz.com/products/test-and-measurement/radome-tester/rs-qar50-quality-automotive-radome-tester_63493-1138625.html, 2019, accessed: Oct. 29, 2024.

[14] O. Oral, T. Feuillen, A. Murtada, and B. S. M. R. Rao, "Fast sparsity-based 3D near-field MIMO imaging using b-SAGA with a batch size selection strategy," in *2025 IEEE Radar Conference (RadarConf25)*, 2025, pp. 751–756.